Journal of Sustainable Development of Energy, Water and Environment Systems

http://www.sdewes.org/jsdewes

Year 2024, Volume 12, Issue 2, 1120486

Original Research Article

Supplementary Controller on Multi-Terminal Direct Current Link for the Damping of Interarea Power Oscillation of Kundur Two-Area Four-Machine System for Sustainable Grid Network

Oluwafemi E. Oni,*[1], Omowunmi M. Longe[1]

[1]Department of Electrical and Electronic Engineering Science, University of Johannesburg, Johannesburg, South Africa

e-mail: 223248712@student.uj.ac.za, omowunmil@uj.ac.za

Cite as: Oni, O., Longe, O. M., Supplementary Controller on Multi-Terminal Direct Current Link for the Damping of Interarea Power Oscillation of Kundur Two-Area Four-Machine System for Sustainable Grid Network, J.sustain. dev. energy water environ. syst., 12(2), 1120486, 2024, DOI: https://doi.org/10.13044/j.sdewes.d12.0486

ABSTRACT

Inter-area power oscillations, a condition where a group of generators in different areas oscillate against each other, are becoming hard to control due to the recent complexity of power systems. This paper aims to enhance the stability of the modified Kundur two-area-four-machine network model, focusing on the implementation of a robust secondary controller on line commutated converter based multi-terminal high voltage direct current systems. This effort is to provide a better sustainable means of power transmission. The proposed solution entails integrating a local generator controller and a robust controller specifically designed to further mitigate inter-area power oscillations. This study conducted three operational scenarios: the local generator controller with double circuits alternating current lines, the local generator controller with multi-terminal direct current system controllers, and the local generator controller with direct current controllers and a secondary controller. Simulation results, executed using electromagnetic transient simulation engine on power systems computer aided design, demonstrated notable improvement in damping inter-area power oscillations with the incorporation of multi-terminal direct current system. A substantial enhancement of 100% in dampening inter-area power oscillations was observed upon implementing a secondary controller on the multi-terminal direct current system.

KEYWORDS

LCC HVDC Multi-terminal DC system, Small signal stability, Interarea power oscillations, Two-Area four machine network, Supplementary controller, VDCL controller.

INTRODUCTION

The proliferation of interconnections within power systems has given rise to inter-area oscillations, where groups of generators oscillate relative to one another—a phenomenon that is challenging to manage due to its scope and intricacy [1]. Characterized by low frequencies, these oscillations pose a significant hurdle to the secure functioning of current power transmission networks. Insufficient damping of inter-area oscillations can precipitate voltage or rotor angle instability, potentially leading to system collapses. Discussions between scholars, electricity utilities, and other industries have long revolved around inter-area oscillations,

* Corresponding author

which typically occur within the frequency broadband of one-tenth to a unit of low frequency [2].

These oscillations either lack sufficient damping or exhibit instability, rendering the network less stable when pivotal faults occur along transmission lines. It often significantly impacts the reliability and effective operation of large-scale interconnected power systems because it limits the loadability of the tie-lines across various zones. Also, because power networks often run close to their maximum install capacity in a deregulated energy market context, inter-area oscillations frequently suffer from insufficient damping.

In the past two decades, power engineers and control researchers have devoted extensive efforts to enhancing the resilience of electricity grid [3]. However, conventional controllers such as the governors' control, automatic voltage regulator (AVR), and power system stabilizer (PSS) being a non-coordinated linear controller with single input and output often fall short in ensuring system stability during significant disturbances or contingencies. Moreover, while AVRs typically maintain synchronous generators (SGs) terminal voltage magnitude, they can introduce negative damping torques, adversely affecting stability. Variations in operating points and disruptions like short circuits cause electromechanical oscillations in power systems. Controlling these frequency oscillations to an acceptable level is crucial; otherwise, their increasing amplitude might lead to instability. To mitigate these challenges, power system stabilizers (PSSs) are employed to generate an additional stabilizing signal for the excitation system, aimed at damping these oscillations [4].

To overcome inter-area oscillation dampening, alternative controllers such as flexible AC transmission systems (FACTS) which comprise divers' static compensators and synchronous condensers have been used. However, in some operational settings, an inter-area mode may be visible from one area while being controllable from another [5, 6]. Under these conditions, a failure or disruption in one region might have a greater impact on another.

Scholars and experts in energy have devised a number of efficient ways for investigating oscillation with a low magnitude of frequency. Modal analysis using linearized state matrices stands as a fundamental approach for assessing low-frequency oscillations, aiding in the identification of oscillation modes with weak damping, either inter- or local. Through uniform participating factors, specific generators' high association with weakly damped modes can be precisely determined. Employing a fuzzy controller allows for swift feedback and integrated control over a broad power network to rapidly damp IAP Oscillations [7]. In [8], a Fractional Order Proportional Integral (FOPI) controller, optimized through an adaptive differential evolution algorithm, was pitted against the conventional PI controller to further fine-tune FOPI performance. Another study implemented a data-enabled prediction technique for optimal damping of wide inter-area power (IAP) oscillations on a voltage source converter (VSC)-based high-voltage DC (HVDC) system [9]. A Wide Area controller for the damping of IAP oscillations has been suggested for power storage devices like capacitors to reduce oscillations at low frequencies [10]. To fine-tune these wide-area controllers, the authors used a particle swarm optimization. Furthermore, in a comparable study described in [11], dual power oscillation dampers were used to dampen IAP oscillations on the power of a double-fed asynchronous induction generators. Renewable energy often contributes harmonics and oscillations in to the grid, especially during systems disturbance. The work in [12] investigated such harmonics contributions using the two area four machine network.

Several research have examined approaches for determining the position and structure of inter-area oscillations, such as the Lyapunov modal analysis framework [13-15]. In addition, research has been undertaken on the dampening of inter-area oscillations in large-scale power systems utilizing decentralized control [16]. The spatio-temporal behaviour of huge interconnected systems in the setting of inter-area oscillations has also been investigated in the literature [17, 18]. Research has also been conducted to damp inter-area oscillations using the Unified Power Flow Controller, considering the role of this technology in damping such oscillations [19]. However, effective damping of inter-area power oscillations in large-scale

power systems has faced several issues. One of the most significant issues is the vast area coverage of power systems, which makes it difficult to determine the sources of inter-region oscillations and adopt efficient damping measures [20]. Usage of long transmission lines and HVDC transmission systems might further increase the likelihood of inter-area oscillations due to increase in harmonics from the HVDC or low short circuit ration of the AC line [21, 22]. Furthermore, implementing damping methods with Unified Power Flow Controllers (UPFCs) might be difficult due to the complexity of the control algorithms and the necessity for correct power system modelling [23-25]. Therefore, undamped inter-area oscillations can cause significant difficulties in power networks, including widespread blackouts.

The identified research gap in the domain of inter-area power oscillation in power systems indicates that creative control solutions have the potential to improve system stability. It is predicted that developing and implementing improved wide-area damping controllers, which use technologies such as machine learning and adaptive algorithms, can effectively attenuate inter-area oscillations, boosting power system stability and reliability. Furthermore, the integration of energy storage systems, notably capacitors, along with enhanced control mechanisms is predicted to result in a significant reduction in low-frequency oscillations. The hypothesis states that filling this research gap will considerably improve the efficiency of power systems in the presence of inter-area power oscillations [26].

Transformations in generation, power transmission trends and grid architecture have resulted from the recent shift toward renewable energy and the broadening of electricity markets, necessitating improved controllers to effectively mitigate inter-area oscillations. Specifically, in operating thyristor-based multi-terminal HVDC systems, it becomes critical to dampen these oscillations before generator controls lose synchronization [27].

This research presents a novel method for modelling a LCC multi-terminal DC (LMTDC) transmission link that provides resilient, flexible, and scalable oscillation damping for a modified Kundur Two Area Four Machine Network (MKTAFMN) system. The approach focuses on constructing and validating a supplementary controller for one of the LMTDC system's rectifying stations. Initially fine-tuned for precise alignment with the MTDC network, this secondary controller is integrated into the LCC-MTDCs (LMTDCs) grid to further enhanced the performance of the voltage dependent current-order limiter (VDCL). This LMTDCs is further complemented with power flow and current sharing control techniques between the rectifier stations and then optimized by the overall controller. Thus, this paper delves into the control strategy of LMTDCs grid, aiming to curtail IAP oscillations within two zones of a transmission networks. This control strategy targets minimizing the adverse impact of faults on AC grid voltage and upholding power balance in the event of an area power imbalance.

The paper's first contribution demonstrates the enhanced stability achievable for two asynchronous grids. The second contribution showcases how unified monitoring and control of a three-terminal LMTDC links can prevent interaction between IAP oscillations from two distinct modes. Through extensive investigation, this study evaluates MKTAFMN performance and proposes robust controller designs to significantly reduce inter-area oscillations, handling voltage control and power oscillation damping simultaneously. A distinctive aspect of this methodology lies in the secondary control's ability to optimize existing rectifier station controls, thus enhancing substation performance. The controller configuration and required parameters are systematically derived from the MKTAFMN model. The suggested secondary control, robust and integrating input-output linearization with nonlinear control methods, dynamically adjusts its parameters, significantly enhancing MTDC controller efficacy in response to varying operational conditions or system structure changes. This paper contributes to significantly to energy sustainability through the proposition of an economically efficient approach to long-distance power transmission. Notably, the study emphasizes the associated advantages of a minimized right-of-way, directly influencing environmental conservation efforts. Furthermore, the integration of multi-terminal high voltage direct current (HVDC) systems results in decreased active power losses, underscoring the significance of this research. The primary focus of the

investigation centers on the incorporation of secondary controllers, showcasing considerable enhancements in the mitigation of power system oscillations within extensive power networks.

The paper's structure encompasses theoretical analysis of IAP oscillations using a two-zone SGs network, presentation of the LMTDC model, elucidation of control architectures encompassing main LMTDC controllers and the supplementary controller, explanation of test system modelling and schematic diagrams, presentation of fault analysis results on the test network, culminating in a comprehensive conclusion summarizing the paper's contributions.

ANALYSIS OF INTER-AREA POWER OSCILLATIONS

Inter-area oscillations pose the greatest risk to the reliability and stability of a synchronously connected power systems [28]. When a the convectional controller, due to low short circuits ratio or weak transmission lines, are unable to fully damp the system's oscillations after a disturbance, it will result in an IAP oscillations [29]. The capacity of an electrical network to remain stable in the presence of this minor perturbations is known as small-signal stability (SSS). When compared to the small signal disturbances, power system, linearization of nonlinear equations around a certain steady-state operating condition is possible. Because of the limited intrinsic damping of IAP oscillations. there is a high likelihood of irreversible, widespread blackouts, which could have catastrophic final impact in terms of the significant economic losses and potential interruption to daily usage of energy.

Eigenvalue analysis, also known as modal analysis, serves as the means to evaluate small-signal stability in power systems. The focus of this study primarily centers on mitigating IAP oscillations. The theoretical underpinning of SSS in power systems is expounded in Equations 1 to 5 below using **Figure 1** which gives a detailed diagram of a two-machine systems. Equations 1 and 2 delineate the swing equation for individual SGs, describing the oscillation of rotor angles δ_a and δ_b in area-A and B, respectively, where H_a and H_b denote the inertias of the generators. The subtraction of these equations yields eq. (3). Further manipulation involves dividing eq. (3) by the respective inertia coefficients before the second derivation, leading to eq. (4), eventually simplified to eq. (5). This analysis aims to ascertain the damping coefficient requisite for effectively mitigating power system oscillations by scrutinizing inertia fluctuations in synchronous machines, indicating the torque necessary for controlling synchronous speed. In the context of stability analysis for extensive systems with numerous synchronized machines, simplifying the swing equations becomes imperative. Combining these equations minimizes the iterations necessary to derive the final swing equations, sidestepping the complexities involved. The summation of the equivalent rotating inertias is determined finding the integral sum of the generator's inertia (H) of each synchronous unit, enabling a comprehensive analysis of the system's stability [30].

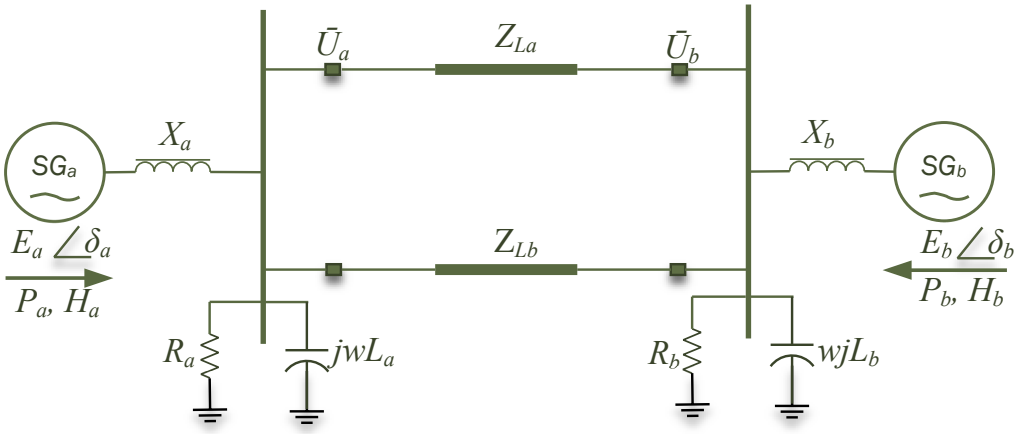

Figure 1. An overview representation of a dual-machines two-area circuits

$$\frac{2}{\omega}H_{\mathrm{a}}\frac{\partial^2\delta_{\mathrm{a}}}{\partial t^2}=P_{\mathrm{ma}}-P_{\mathrm{ea}} \tag{1}$$

$$\frac{2}{\omega}H_{\mathrm{b}}\frac{\partial^2\delta_{\mathrm{b}}}{\partial t^2}=P_{\mathrm{mb}}-P_{\mathrm{eb}} \tag{2}$$

$$\frac{2}{\omega}\left(\frac{\partial^2(\delta_{\mathrm{a}}-\delta_{\mathrm{b}})}{\partial t^2}\right)=\left(\frac{P_{\mathrm{ma}}-P_{\mathrm{ea}}}{H_{\mathrm{a}}}-\frac{P_{\mathrm{mb}}-P_{\mathrm{eb}}}{H_{\mathrm{b}}}\right) \tag{3}$$

$$\frac{2}{\omega}\left(\frac{H_{\mathrm{a}}H_{\mathrm{b}}}{H_{\mathrm{a}}+H_{\mathrm{b}}}\right)\left(\frac{\partial^2(\delta_{\mathrm{a}}-\delta_{\mathrm{b}})}{\partial t^2}\right)=\left(\frac{P_{\mathrm{ma}}H_{\mathrm{b}}-P_{\mathrm{mb}}H_{\mathrm{a}}}{H_{\mathrm{a}}+H_{\mathrm{b}}}-\frac{P_{\mathrm{ea}}H_{\mathrm{b}}-P_{\mathrm{ea}}H_{\mathrm{b}}}{H_{\mathrm{a}}+H_{\mathrm{b}}}\right) \tag{4}$$

$$\frac{2}{\omega}H_{\mathrm{ab}}\frac{\partial^2\delta_{\mathrm{ab}}}{\partial t^2}=P_{\mathrm{mab}}-P_{\mathrm{eab}} \tag{5}$$

The disparity in degree of rotor tilt between the two generators, denoted as H_{ab}, along with δ_{ab} as expressed in eqs. (6) and (7) respectively, signify the relationship between the corresponding inertia constants. The electrical (P_{mab}) and mechanical (P_{eab}) powers exchanged between these generators are captured in eqs. (8) and (9) respectively. The swing characteristics of the synchronous machine are encapsulated by the damping constant $\mathrm{K_D}$, detailed through a second-order differential equation in equation (10). Eqs. (11) and (12) yield the undamped natural frequency (ω_{n}) and the requisite damping coefficient (ζ) crucial for effectively attenuating oscillation amplitudes. The relationship between the frequency of oscillations and constant of inertia indicates that a dynamic network having a higher inertia constant is more resilient to faults, while conversely, demonstrating the direct influence of supplied power output on the system's inertia constant. Thus, enhancing the power system's stability criterion needs an inertia constant exceeding 3.5 pu.

$$H_{\mathrm{ab}}=\frac{H_{\mathrm{a}}H_{\mathrm{b}}}{H_{\mathrm{a}}+H_{\mathrm{b}}} \tag{6}$$

$$\delta_{\mathrm{ab}}=\delta_{\mathrm{a}}-\delta_{\mathrm{b}} \tag{7}$$

$$P_{\mathrm{mab}}=\frac{P_{\mathrm{ma}}H_{\mathrm{b}}-P_{\mathrm{mb}}H_{\mathrm{a}}}{H_{\mathrm{a}}+H_{\mathrm{b}}} \tag{8}$$

$$P_{\mathrm{eab}}=\frac{P_{\mathrm{ea}}H_{\mathrm{b}}-P_{\mathrm{eb}}H_{\mathrm{a}}}{H_{\mathrm{a}}+H_{\mathrm{b}}} \tag{9}$$

$$\frac{2}{\omega}H_{\mathrm{ab}}\frac{\partial^2\delta_{\mathrm{ab}}}{\partial t^2}+\mathrm{K_D}\frac{\partial\delta_{\mathrm{ab}}}{\partial t}+P\cos(\delta_{\mathrm{o}})_{\mathrm{ab_{max}}} \tag{10}$$

$$\omega_{\mathrm{n}}=\sqrt{\frac{\omega P\cos\delta_{\mathrm{omax}}}{2H_{\mathrm{ab}}}} \tag{11}$$

$$\zeta={}^{1}\!/_{2}\,K_{\mathrm{D}}\sqrt{\frac{\omega}{2H_{\mathrm{ab}}P\cos\delta_{\mathrm{omax}}}} \tag{12}$$

MULTI-TERMINAL DIRECT CURRENT MODEL

The LMTDC system utilized in this investigation integrates a three-terminal thyristor converter. Control over the DC voltages (DCV) is managed via the manipulation of firing angles at both rectifiers and converter units. The overarching power controllers are responsible for computing the input DC current (DCC) values allocated to each converter station. The expressions governing the DCV at the inverter and rectifier stations, along with the rectifier firing angle, are detailed in references [31-33]:

$$V_{\mathrm{dr}} = \frac{3\sqrt{2}}{\pi} BTU_{\mathrm{r}} \cos\alpha_{\mathrm{r}} - \frac{3}{\pi} BX_{\mathrm{C}} I_{\mathrm{dc}} \tag{13}$$

$$V_{\mathrm{di}} = \frac{3\sqrt{2}}{\pi} BTU_{\mathrm{i}} cos\beta_{\mathrm{i}} + \frac{3}{\pi} BX_{\mathrm{C}} I_{\mathrm{dc}} \tag{14}$$

$$\alpha_{\mathrm{r}} = \cos^{-1}\left(\frac{I_{\mathrm{dcref}} R_{\mathrm{dc}} + U_{\mathrm{dci}} + {}^{3}/_{\pi}\, BXI_{\mathrm{dcref}}}{BTU_{\mathrm{r}} {}^{3\sqrt{2}}/_{\pi}}\right) \tag{15}$$

Eqs. (13) to (15) feature subscripts i and r representing inverter or rectifier respectively. Within these equations, V_{di} and V_{dr} symbolize the DCV of the inverter and rectifier, while U denotes the RMS line-to-line voltage. The series arrangement of the thyristor bridges is designated as B. Specifically, for a 12-pulse thyristor converter, B equals 2, whereas a bipolar system would possess a B=4. The parameter α corresponds to the firing angle for the rectifier circuits. Additionally, X signifies the commutation reactance, R_{dc} defines the aggregate resistance of the converter, and T denotes turns ratio of the transformer.

MULTI-TERMINAL DIRECT CURRENT CONTROLLER

The conventional control strategy for LMTDC converters necessitates the rectifier station to operate in DCC mode, while the inverter station employs VDCL, extinction angle control (EAC), and current control. Illustrated in Figure 2, the DCC method at the rectifier is contrasted by comparing the current order from VDCL with the filtered DC current derived from the overall power controller's measured DC power, yielding the reference current order (I_{order}). The lower value between these two sets the standard I_{order} for the rectifier's firing angle generation. In the same Figure 2 depiction, diverse control strategies are available for the inverter, including EAC, DCC, and DCV control. Similar to the rectifier, the reference value is obtained using a similar methodology. However, the discrepancy between the typical current order and the current margin (I_{dcmarg}) restricts the inverter's DC current. To positively impact the power reversal process, I_{dcmarg} is incorporated into the inverter's current control, conventionally established within a predefined range spanning 0.1 to 0.15 pu. Ordinarily, a current error control (I-error) intervenes between DCC and DVC, facilitating smoother transitions amid control modes. To enhance smoothness in transitions, this derived I-error can also be introduced between DCC and EAC. Opting for the smallest among these produced parameters is advantageous for inverter control. Operating the inverter at the minimum extinction angle diminishes power losses, curtails reactive power necessities for compensating thyristor valves, and ultimately diminishes harmonic distortion content. Each input in this control signal, conveyed in per units, undergoes a first-order inertia transfer function, ensuring seamless transitions during control switching. This procedural mechanism is mathematically articulated as:

$$G\,\frac{1}{1+sT} \tag{16}$$

The Supplementary Controller (SC) employed in this work resembles a POD, sharing a construction similar to a generator's PSS. It comprises a washout filter, a gain factor *G* and *p* phase lead-lag, as depicted in **Figure 2**. Eq. (16) defines the transfer function governing the secondary controller. In practical application, the washout filter serves as a crucial intermediary within the control loop, aiming to filter out the steady-state component from the measured signal while preserving transient components. The conventional design tuning methodology involves two primary steps:

i) Determining *T4* and *T5* to amend the phase of the residual mode to 180 degrees.

ii) Fine-tuning the gain factor *G* to attain the desired damping effect.

$$H_{\mathrm{sc}} = \left(G1\frac{1}{1+sT1}\right)\left(G2\frac{sT2}{1+sT3}\right)\left(G3\frac{1+sT4}{1+sT5}\right)^{\mathrm{p}}\left(G4\frac{1}{1+sT6}\right) \quad (17)$$

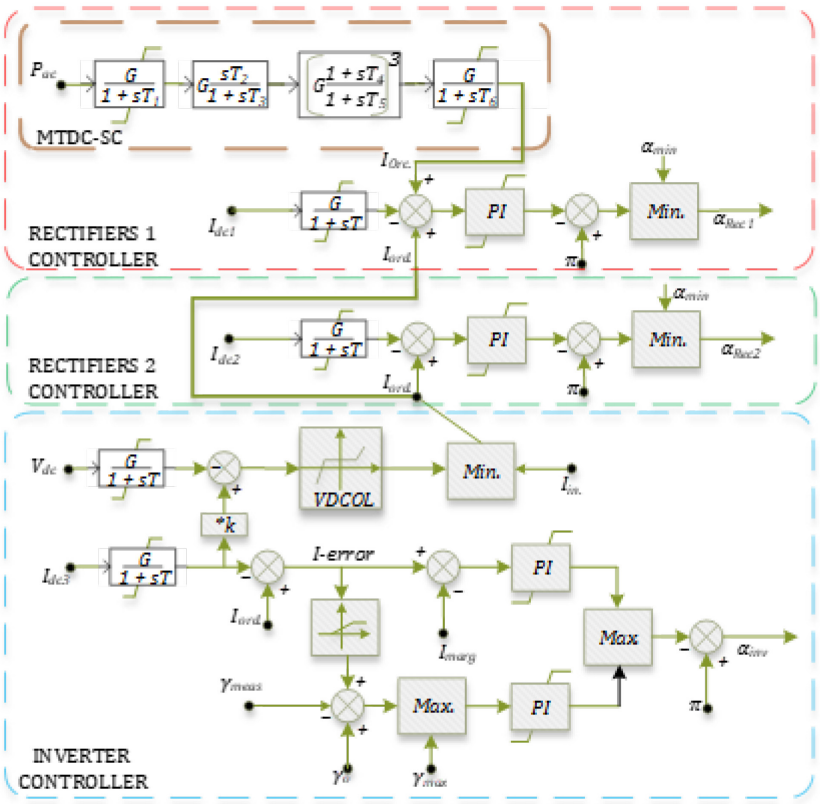

Figure 2. LMTDC controller design for all converter station

The fault susceptibility of the LMTDC system hinges significantly on its overall coordination, prompting the pre-configuration and adjustment of each converter's controllers tailored to the specific case study under consideration. Oversight and regulation of the LMTDC link's converter operations fall under the purview of the overarching power controller. This controller generates an output by adjusting the power order obtained from the systems, subsequently deriving the I-order by dividing it with the measured DCV. Maintaining a balanced total DCC across all converters at zero (I_{dc}=0) remains a primary objective. The master control, depicted in **Figure 3**, assumes responsibility for harmonizing the aggregated power and current orders across the converters. It formulates the I-order for all the converters, accounting for measured voltages at individual converter stations and predetermined power orders. Additionally, this controller incorporates allowances and compensations to mitigate losses along the DC lines.

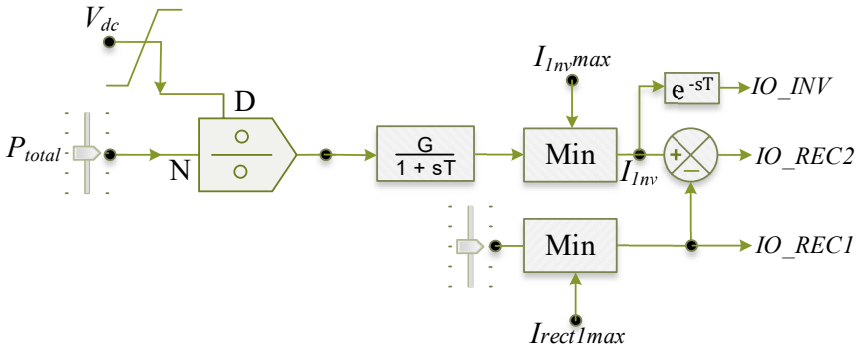

Figure 3. Overall power Controller

MODELLING OF THE TEST SYSTEM

The study system considered in this paper is a MKTAFM network as shown in **Figure 4**. The study network consists of 4 generators, located in two areas, a three-terminal LMTDC line and both DC and AC lines. The deployed SGs additionally include a type 4 IEEE exciter for the AVR and a PSS. The transmission line interconnecting B10 to B11 was modified from 25 km to 80 km distance, and as a result, had a large line impedance. A double circuits transmission line is therefore used to enable more power transfer across area-A and B. Thus, the complete generator's IAP and frequency oscillations were then analyzed utilizing a real-time domain simulation. Two faulty methods were put in place to mimic a worst-case condition. The power for each generating unit, synchronous speed, and inter-area power transmission was plotted during this system disturbance. Buses B7, B8, and B9 were chosen to evaluate the power transfer quality and voltage profile throughout this station. The aforementioned mode is inter-area because it consists of two coherent pairs of generators swinging at low speeds against one another.

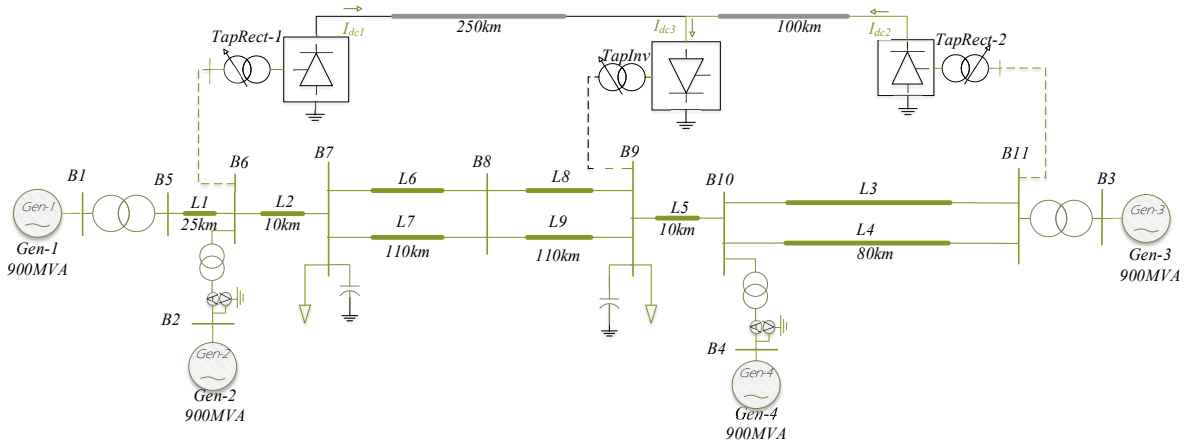

Figure 4. The modified Kundur two-area four-machine network (MKTAFMN)

The synchronous machines in the system were modeled using PSCAD, incorporating the IEEE controller models for AVR and PSS. Each generator's true inertial constant was assessed, interconnected via a 20/230 kV step-up transformer with an power rating of 900 MVA with capability of giving 700 MW true power. For evaluation purposes, the same value of control parameters was uniformly assigned to the SGs control across all four machines to thoroughly analyse the impact of the LMTDC controller in mitigating disturbances arising from faults within the comprehensive model. The modelling specifics for these machines were elucidated by the authors in **[10]**, documented in Table 1 within the Appendix section. Dynamic simulations of the network encompassed three operational scenarios:

- Sole utilization of the AC line within the MKTAFMN model.
- Integration of the LMTDC system connecting bus B6 (Rect-1), B11 (Rect-2) to the inverter link at bus B9.
- Introduction of a supplementary controller specifically on the rectifier 1 converter.

Single transmission line was utilized during the second and third scenarios, instead of the double lines in the original MKTAFN model. This decision was made to prevent excess power transmission from the SGs to the load which might give an incorrect picture of the entire network, but to adequately highlight the impact of changing an older installed AC transmission line with an alternative DC line, hence demonstrating the whole system's outcome.

RESULTS AND ANALYSIS

A dynamic RMS simulation was conducted on the MKTAFM model to investigate its small-signal characteristics. The simulation encompassed a scenario involving a three-phase to ground (3P-G) fault occurrence on the L7 line, linking B7 and B8, with a fault and the faults was cleared at time t=130 ms, concurrent with a disturbance lasting 1.0 second on Gen-4, both events coinciding at the 2.0-second time. This orchestrated dual disturbance aimed to stress different facets of the system, providing a rigorous assessment of power system operation limits, portraying a worst-case scenario. In subsequent scenarios, the same fault impedance was imposed on the system while connected to the LMTDC model, allowing an evaluation of LMTDC transmission methodologies' impact on electric power system stability.

PSCAD/EMTDC software was used to run the dynamic simulation for the entire network. Observations were focused on the SGs active power and oscillation speed followed by the magnitude and damping rate of oscillations, particularly the IAP oscillations, to discern the contribution of each SGs in the oscillatory phases. Despite exhibiting distinct amplitudes and waveform distortion, both situations maintained a stable operational state following system disruption, benefiting from a positive damping coefficient.

Figure 5 illustrates the real power generated by all SGs across the three case studies. In the first scenario, SG 2 (Gen-2) experienced the lowest power dip, reaching 201 MW during the 3P-G fault occurrence due to the close distance to the fault. Subsequently, Gen-1 exhibited a similar dip. The decline in active power from Gen-3, nearing 1 second in simulation time, led to Gen-4 producing 1075 MW, approximately 1.54 pu of its operating state value. Gen-3 and Gen-4, sharing similarities in Area B, followed a comparable pattern. Additionally, an inconsistency in generated power among the generators was noted, with Gen-4 contributing the most to the load power, followed by Gen-2 and Gen-1. This variance was attributed to the high impedance from the AC line occurring between Gen-3 and the load area, highlighting limitations in power controllability within AC generation systems.

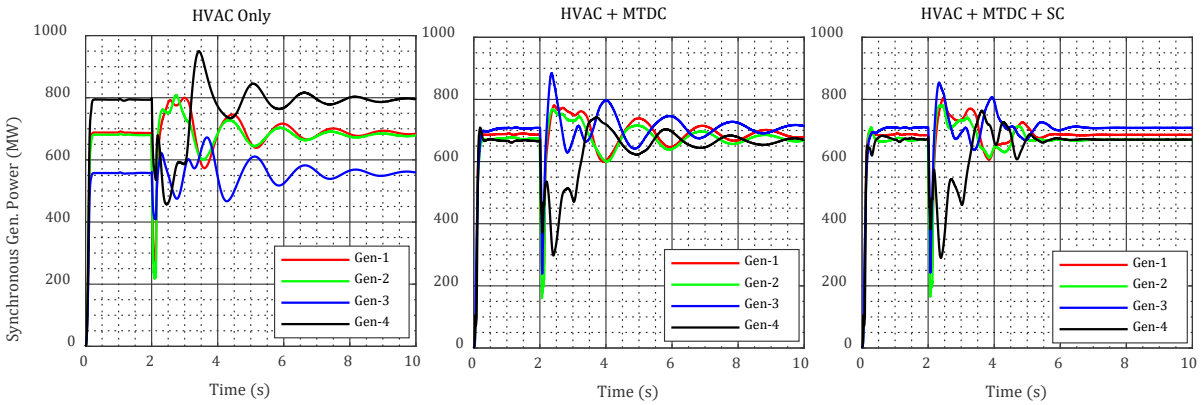

Figure 5. Active power generated by each synchronous generator

The second scenario entailed substituting all dual transmission circuits with a single circuits line and the LMTDC line. A comparative performance evaluation was conducted against the original case study to determine the superior approach in mitigating inter-area oscillations. During system disturbances, the subplot depicting active generator power in **Figure 5** exhibited reduced power swings. Following the 3P-G fault, Gen-4 and Gen-3, experiencing prolonged generator faults, registered the highest power amplitudes, reaching 905 MW. These amplitudes significantly led to a larger inertia value, allowing the network's restoration to its base case. In contrast, Gen-2 still had the highest SG dip, at 195 MW. Notably, the power profile in this scenario demonstrated a better-balanced power output across all four generators. These balanced results were obtainable by the addition of the LMTDC model, which improved active power dispatch. However, some residual oscillations were still visible in the simulation plots at this point. Upon introducing the supplementary controller to the rectifier 1 converter's controller led to an increase in the SG inertia which further helps in the total eradication of all the oscillations by 4.5 seconds into the simulation.

Figure 6 depicts the observed frequency swings among the four SG within the system. This outcome involves incoherent machines, where area-A has a different constant of inertia than area-B, leading to synchronization issues between generators in these respective areas. Notably, the highest IAO, reaching up to 1.006 pu, were recorded in the Gen-1 and Gen-2 plots. These machines' increased power dynamics in area-A were critical in satisfying the load demand in area-B, sustaining a stable operational state despite the elevated oscillating frequency. The AVR and PSS controllers for the SGs have offered a more damping torque for the systems in the first two cases, with the goal of maintaining a stable operating point. Nevertheless, these efforts were unsuccessful in establishing a damping coefficient quickly enough to properly restore the complete test network to its steady-state operating condition. Further increase in the fault clearing time (t_c) of 200 ms resulted in system collapse, in which the systems are unable to maintain a stable operational point.

While the initial oscillation in the third case study matched that of the others, the integration of the secondary controller into the KMTAFMN model quickly provided a significant dampening torque. This aided the system's quick restoration to its stable original conditions.

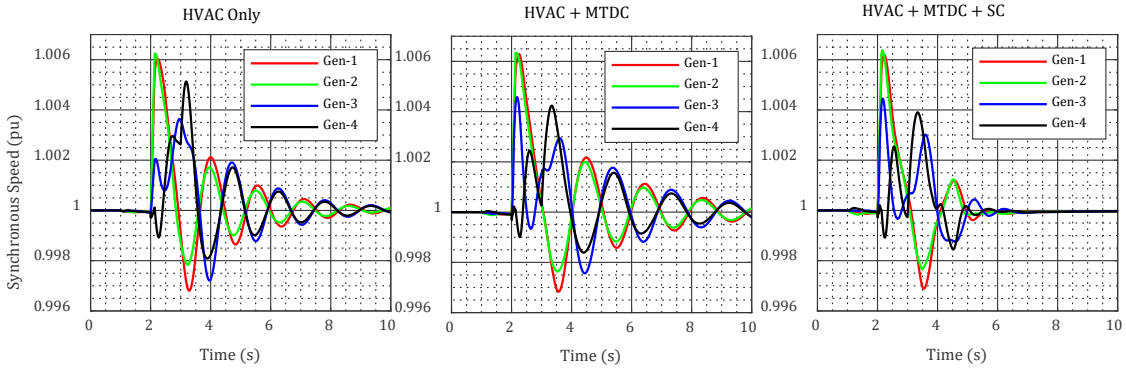

Figure 6. Synchronous speed

Following the disturbance, the bus voltages at B7, B8, and B9 (depicted in **Figure 7**) represent the observed voltage profiles across various scenarios. The findings show that B8 is the most vulnerable bus in the network in all the three case studies, owing to its significant distance from the SGs in both zones followed by B7 which was identified as the next weak bus based on distance to the SGs as well. Nonetheless, the voltage profile in the second scenario displayed an enhanced performance compared to the sole utilization of HVAC lines. In both instances, increasing the transmission distance connecting B10 and B11 had a very little impact on B9's voltage profile compared to the other investigated buses. The voltage profile fluctuations recorded in the system were completely corrected during the third case study of utilizing a supplementary controller, and thus further stabilizing the system's steady state operational condition within about one cycle. (equivalent to 4.5 seconds time of simulation).

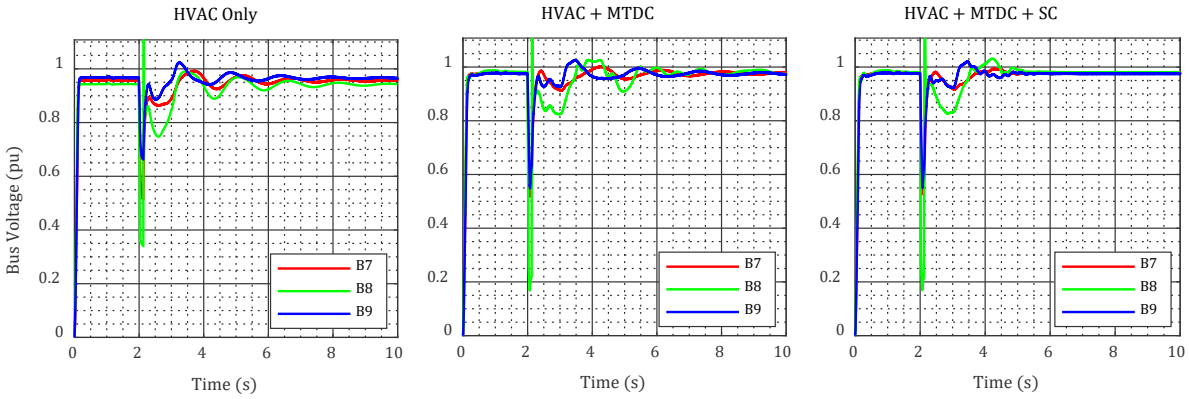

Figure 7. Bus voltage profile

Further simulation shown in **Figure 8** described the performances of all the SGs during all the three case studies. The first subplots are the load angle which ranges between 50 and 55 for all the SGs. Oscillations after fault has been cleared can be observed in both first and second case study but was well damped in the third case study. However, inclusion of LMTDC into the systems lead to high harmonics in the load angle plots for both last case study. The normalised field voltage and the SGs phase angles are shown next which all point to the improvements recorded after using the supplementary controller in the third case study. **Figure 9** shows the LMTDC data for the last two case studies. The converter power shows 200 MW, 485 MW and 680 MW for rectifier 1, rectifier 2 and inverter respectively. Third case study shows how active power was added through the inclusion of the supplementary controller which added to the current order to further help in the quick damping of the IAP oscillations. The firing angle, the DCC, DCV (475 kV) and VDCL is further shown in this plot.

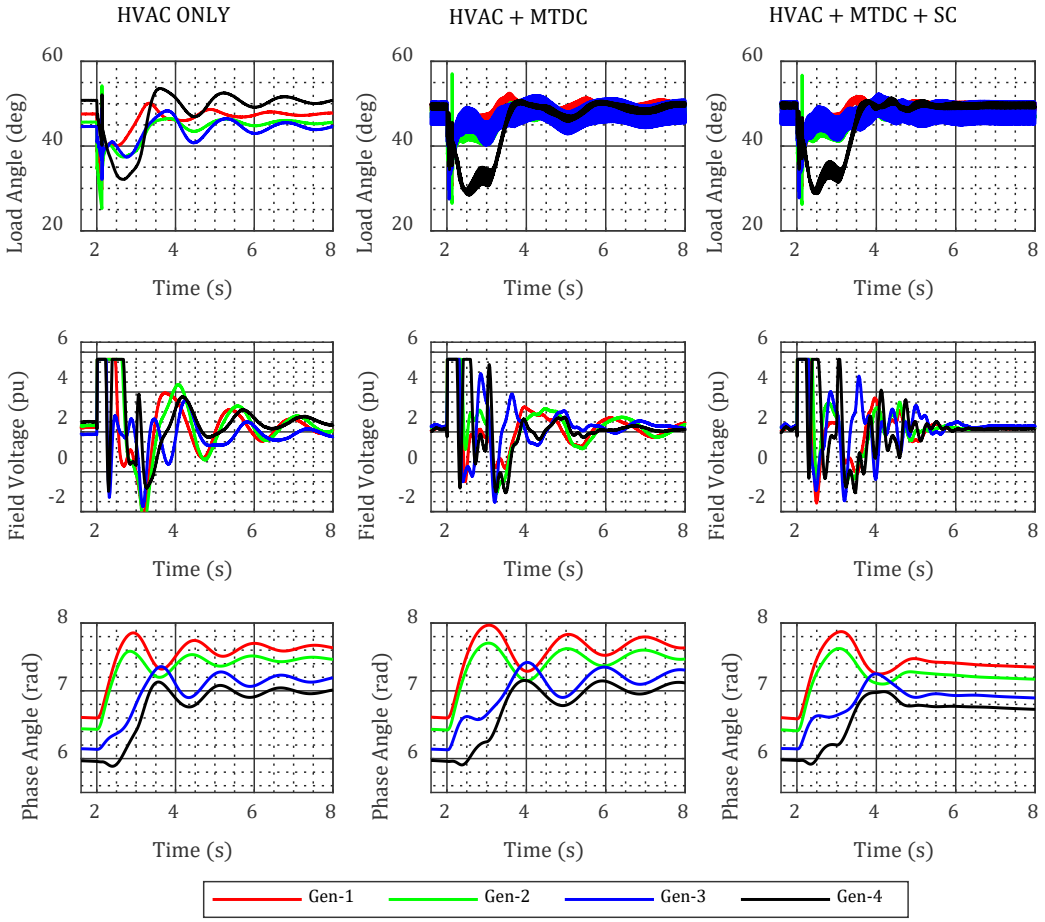

Figure 8. SGs detailed results based on the three case studies.

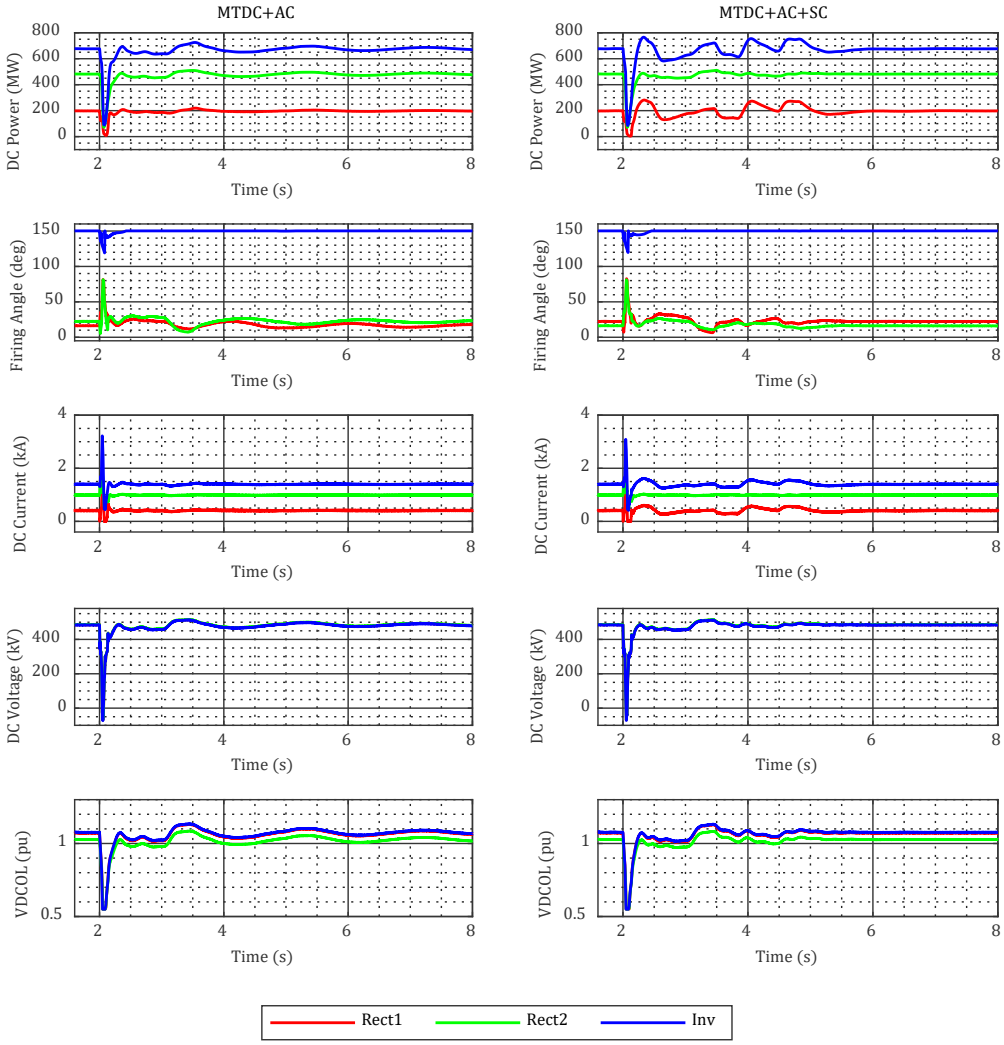

Figure 9. LMTDC detailed results when in operation for second and third case studies

The supplementary control data is shown in **Figure 10**. The input of this controller is from the difference in the power reference across the inter-area lines. Each of the lines in this plot shows the output from each of the control block. The final signals, SC_{in}, was then added to the current order which is further used in generating the firing angle for the rectifier 1 substation.

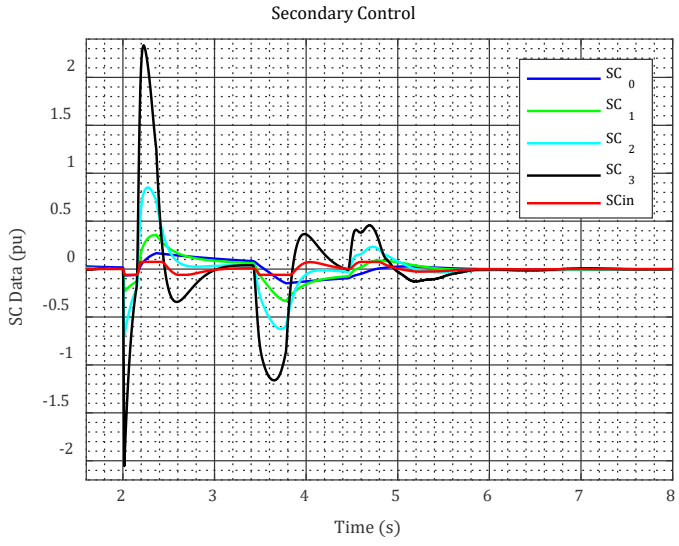

Figure 10. Supplementary control signals

Figure 11 illustrates the IAP transfer dynamics between busbar B7 and B9. In the absence of LMTDC links, the first case study solely employing AC transmission lines, revealing a very slow damping of the IAP oscillations. During the post-fault state, both zones significantly contribute to these oscillations, impeding the system's prompt return to the original operating condition. However, upon integrating the MTDC link, notable enhancement in the damping rate of IAP oscillations was observed during the same scenario. This upgrade led to a substantial positive damping rate in the amplitude of the IAP transfer, resulting in a more stabilized operational condition. Yet, despite these improvements, complete damping of all IAO was not achieved by the 8-second mark of the simulation. To address this, a secondary controller was introduced, showcasing improved oscillation damping whereby all oscillations were completely quelled precisely at 4.5 seconds into the simulation. The active power transfer in this scenario consisted of power delivered from AC line L6 to line L8 and the LMTDC power transmitted via the Rect-1 converter connection. The presented data shows a damping ratio that entirely reduced the oscillation amplitude's value during the simulation's later phase.

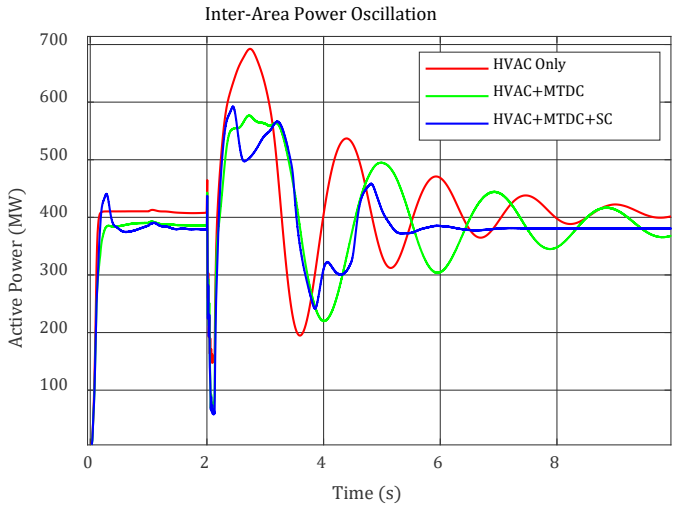

Figure 11. Inter-area power transfer for each scenario considered

CONCLUSION

Power utilities continue to face substantial challenges due to the modest signal stability issue of two asynchronous machines. This work proposed a hierarchical control strategy for improving inter-area oscillation damping stability. The comprehensive solution encompasses indigenous controllers from the synchronous generators (SGs), exciters and speed control, a centralized power controller for the LMTDC system, and the current and extinction angle control within the LMTDC model. These integrated controllers were strategically used to improve system performance.

The base case study involved building a dynamic simulation model of an MKTAFMN (Modified Kundur Two-Area Four-Machine Network) model. The fault scenario included a disturbance at Gen-4 and a 130 ms 3P-G fault on system line L6, which connected B7 to B8, both of which occurred 2 seconds into the exercise. Thirdly, the system response was analyzed, monitoring generator details on a plot and determining instances of high waveform imbalance, and the time required for synchronous generators (SGs) control to dampen system inter-area oscillations efficiently. Following that, a case study replaced the network's double transmission lines with an LMTDC system (second case study), followed by the installation of a supplementary control to the LMTDC (third case study).

A nonlinear time-domain dynamics analysis was conducted on the LMTDC network, monitoring generator behaviour and bus voltage profiles. Following the 3P-G fault on the test network, examination of the least damped modes in each grid study affirmed that implementing the secondary controller on the LMTDC achieved 100% damping of oscillations with zero

amplitude change rates compared to the initial and subsequent scenarios. These results demonstrate the robustness of the proposed controller, significantly elevating the system's stability limit and enhancing primary controller performance. One vital goal of this study is that it facilitates the integration of renewable energy sources, such as wind and solar, by reducing the intermittent oscillations and efficiently transmitting power from remote renewable-rich areas to demand centres. This enhances the utilization of clean energy and supports the transition to a more sustainable and low-carbon energy mix.

Future research will focus on reducing the controller's sensitivity to substantial and non-uniform transmission delays and exploring its effects when implemented in other LMTDC substations.

NOMENCLATURE

Abbreviations

MKTAFM	Modified Kundur Two-Area-Four-Machine
PSSs	Power System Stabilizers
AVR	Automatic Voltage Regulator
VSC	Voltage Source Converter
LCC	Line Commutated Converter
FOPI	Factional Order Proportional Integral
G	Gain
PI	Proportional and Integra
MTDC	Multi-terminal High Voltage Direct Current
FACTS	Flexible AC Transmission Systems
WADC	Wide Area Damping Controller
LMTDC	LCC MTDC
VDCL	Voltage Dependent Current-order Limiter
I_{order}	The reference current order
EAC	Extinction Angle Control
I_{dcmarg}	Current margin
I-error	Current error control

REFERENCES

1. S. Sitompul and G. Fujita, "Impact of State-of-Charge Control Integrated with Load-Frequency Control on Battery Energy Storage System in Islanded Microgrid System," in 2021 IEEE 12th Energy Conversion Congress & Exposition-Asia (ECCE-Asia), 2021: IEEE, pp. 199-203, https://doi.org/10.1109/ECCE-Asia49820.2021.9479179.
2. M. Klein, G. J. Rogers, and P. Kundur, "A fundamental study of inter-area oscillations in power systems," IEEE Transactions on power systems, vol. 6, no. 3, pp. 914-921, 1991, https://doi.org/10.1109/59.119229.
3. J. Machowski, Z. Lubosny, J. W. Bialek, and J. R. Bumby, Power system dynamics: stability and control. John Wiley & Sons, 2020.
4. J. Shair, H. Li, J. Hu, and X. Xie, "Power system stability issues, classifications and research prospects in the context of high-penetration of renewables and power electronics," Renewable and Sustainable Energy Reviews, vol. 145, p. 111111, 2021, https://doi.org/10.1016/j.rser.2021.111111.
5. R. Huang, W. Gao, R. Fan, and Q. Huang, "A guided evolutionary strategy based static var compensator control approach for inter-area oscillation damping," IEEE Transactions on Industrial Informatics, 2022, https://doi.org/10.1109/TII.2022.3177430.

6. R. Huang, W. Gao, R. Fan, and Q. Huang, "Damping inter‐area oscillation using reinforcement learning controlled TCSC," IET Generation, Transmission & Distribution, vol. 16, no. 11, pp. 2265-2275, 2022, https://doi.org/10.1049/gtd2.12441.
7. K. Sreedivya, P. A. Jeyanthy, and D. Devaraj, "Improved design of interval type-2 fuzzy based wide area power system stabilizer for inter-area oscillation damping," Microprocessors and Microsystems, vol. 83, p. 103957, 2021, https://doi.org/10.1016/j.micpro.2021.103957.
8. S. S. Biswal, D. R. Swain, and P. K. Rout, "Inter-area and intra-area oscillation damping for UPFC in a multi-machine power system based on tuned fractional PI controllers," International Journal of Dynamics and Control, vol. 10, no. 5, pp. 1594-1612, 2022, https://doi.org/10.1007/s40435-021-00891-4.
9. L. Huang, J. Coulson, J. Lygeros, and F. Dörfler, "Decentralized data-enabled predictive control for power system oscillation damping," IEEE Transactions on Control Systems Technology, vol. 30, no. 3, pp. 1065-1077, 2021, https://doi.org/10.1109/TCST.2021.3088638.
10. A. Prakash, K. Kumar, and S. Parida, "Energy capacitor system based wide-area damping controller for multiple inter-area modes," IEEE Transactions on Industry Applications, vol. 58, no. 2, pp. 1543-1553, 2022, https://doi.org/10.1109/TIA.2022.3140713.
11. S. Alalwani, S. Isik, and S. Bhattacharya, "Inter-area Oscillation Damping Controller for DFIG based Wind Power Plants," in 2022 IEEE Energy Conversion Congress and Exposition (ECCE), 2022: IEEE, pp. 1-6, https://doi.org/10.1109/ECCE50734.2022.9947750.
12. O. E. Oni and O. M. Longe, "Analysis of secondary controller on MTDC link with solar PV integration for inter-area power oscillation damping," Energies, vol. 16, no. 17, p. 6295, 2023, https://doi.org/10.3390/en16176295.
13. A. B. Iskakov, E. Y. Kutyakov, N. V. Tomin, D. A. Panasetsky, A. N. Abramenkov, and S. V. Dushin, "Estimation of the location of inter-area oscillations and their interactions in electrical power systems using Lyapunov modal analysis," International Journal of Electrical Power & Energy Systems, vol. 153, p. 109374, 2023, https://doi.org/10.1016/j.ijepes.2023.109374.
14. A. B. Iskakov and I. B. Yadykin, "Lyapunov modal analysis and participation factors applied to small-signal stability of power systems," Automatica, vol. 132, p. 109814, 2021, https://doi.org/10.1016/j.automatica.2021.109814.
15. W. Han and A. M. Stanković, "Model-Predictive Control Design for Power System Oscillation Damping via Excitation-A Data-Driven Approach," IEEE Transactions on Power Systems, vol. 38, no. 2, pp. 1176-1188, 2022, https://doi.org/10.1109/TPWRS.2022.3177561.
16. C. Zhang, D. Ke, Y. Sun, C. Chung, and J. Xu, "Investigations of large-scale voltage-dependent loads for damping inter-area oscillations: Mechanism and robust decentralized control," IEEE Transactions on Power Systems, vol. 33, no. 6, pp. 6037-6048, 2018, https://doi.org/10.1109/TPWRS.2018.2854648.
17. H. Pulgar-Painemal, Y. Wang, and H. Silva-Saravia, "On inertia distribution, inter-area oscillations and location of electronically-interfaced resources," IEEE Transactions on Power Systems, vol. 33, no. 1, pp. 995-1003, 2017, https://doi.org/10.1109/TPWRS.2017.2688921.
18. L. Zhu et al., "Mitigating Inter-Area Oscillations Using Adaptive Wide-Area Damping Controller Based on Measurement-Driven Model: Case Studies on Realistic Grid Models and Actual Events," CIGRE general session 2020, 2020.
19. P. He, S. A. Arefifar, C. Li, F. Wen, Y. Ji, and Y. Tao, "Enhancing oscillation damping in an interconnected power system with integrated wind farms using unified power flow controller," Energies, vol. 12, no. 2, p. 322, 2019, https://doi.org/10.3390/en12020322.

20. R. A. Biroon, P. Pisu, and D. Schoenwald, "Inter-area oscillation damping in large-scale power systems using decentralized control," in Dynamic Systems and Control Conference, 2018, vol. 51906: American Society of Mechanical Engineers, p. V002T19A005.
21. A. M. Vural, "Contribution of high voltage direct current transmission systems to inter-area oscillation damping: A review," Renewable and Sustainable Energy Reviews, vol. 57, pp. 892-915, 2016, https://doi.org/10.1016/j.rser.2015.12.091.
22. G. Arcia-Garibaldi, P. Cruz-Romero, and A. Gómez-Expósito, "Future power transmission: Visions, technologies and challenges," Renewable and Sustainable Energy Reviews, vol. 94, pp. 285-301, 2018, https://doi.org/10.1016/j.rser.2018.06.004.
23. P. Jiang, Z. Fan, S. Feng, X. Wu, H. Cai, and Z. Xie, "Mitigation of power system forced oscillations based on unified power flow controller," Journal of Modern Power Systems and Clean Energy, vol. 7, no. 1, pp. 99-112, 2019, https://doi.org/10.1007/s40565-018-0405-5.
24. E. Solomon et al., "Mitigating Low-Frequency Oscillations and Enhancing the Dynamic Stability of Power System Using Optimal Coordination of Power System Stabilizer and Unified Power Flow Controller," Sustainability, vol. 15, no. 8, p. 6980, 2023, https://doi.org/10.3390/su15086980.
25. R. Adapa, S. L. Nilsson, B. R. Andersen, and Y. Yang, "Technical Description of the Unified Power Flow Controller (UPFC) and Its Potential Variations," Flexible AC Transmission Systems: FACTS, pp. 299-351, 2020, https://doi.org/10.1007/978-3-030-35386-5_10.
26. I. Zenelis, Inter-area oscillations in power systems with uncertainties: data-driven wide-area damping control design and monitoring enhancement using energy storage. McGill University (Canada), 2021.
27. F. Ahmed, A. Foley, S. McLoone, R. J. Best, C. Cameron, and D. Al Kez, "Dynamic grid stability in low carbon power systems with minimum inertia," Renewable Energy, 2023, https://doi.org/10.1016/j.renene.2023.03.082.
28. S. Eberlein, Small-Signal Stability Modelling and Optimization of Microgrids. BoD-Books on Demand, 2021.
29. O. E. Oni, A. G. Swanson, and R. P. Carpanen, "Small signal stability analysis of a four-machine system with placement of multi-terminal high voltage direct current link," Journal of Energy in Southern Africa, vol. 31, no. 1, pp. 73-87, 2020, https://doi.org/10.17159/2413-3051/2020/v31i1a7430.
30. X. Zou, "Frequency and damping characteristics of generators in power systems," Virginia Tech, 2018.
31. M. Faruque, Y. Zhang, and V. Dinavahi, "Detailed modeling of CIGRE HVDC benchmark system using PSCAD/EMTDC and PSB/SIMULINK," IEEE transactions on power delivery, vol. 21, no. 1, pp. 378-387, 2005, https://doi.org/10.1109/TPWRD.2005.852376.
32. O. E. Oni, A. G. Swanson, and R. P. Carpanen, "Modelling and control of multiterminal LCC HVDC," in 2018 IEEE PES/IAS PowerAfrica, 2018: IEEE, pp. 274-279.
33. M. Mankour and B. S. Sami, "Mitigation of commutation failure method in LCC converter based on HVDC systems by mean of modeling and simulation," Journal of Ambient Intelligence and Humanized Computing, pp. 1-16, 2020, https://doi.org/10.1007/s12652-020-01924-0.

APPENDIX

	Rect-1	Rect-2	Invtr
Rated power in MW	300/200	1000/500	1200/700
Rated DC current in kA	0.3/0.2	1.0/0.5	1.2/0.75
Firing angle for the converter	14.8	18	15
	6 pulse thyristors transformer rating		
Power rating in MVA	400	1000	1400
Voltage rating in kV	230/500	230/500	500/230
Transformer reactance in pu	0.18	0.18	0.18
	PI Controller		
Gain	1.099	1.536	1.536
Controller time constant in s	0.01093	0.01525	0.01525
	VDCOL		
Input threshold value	0.4-1.0	0.4-0.9	0.4-0.9
Output threshold value	0.53-1.52	0.53-1.0	0.53-1.0
T-model for DC Transmission line		AC Transmission line	
R(Ω/km)	0.01	r (pu/km)	0.0001
Reactor (H)	0.5968	x_L (pu/km)	0.001
DC filter (uF)	15	b_c (pu/km)	0.00175

Paper submitted: 26.11.2023
Paper revised: 06.02.2024
Paper accepted: 07.02.2024